Order and Disorder in Niobium Tungsten Oxides of the Tetragonal Tungsten Bronze Type

Frank Krumeich

Laboratory of Solid State Physics, ETH Zürich, CH-8093 Zürich, Switzerland. E-mail: krumeich@solid.phys.ethz.ch

Abstract

Two superstructures of the TTB type (tetragonal tungsten bronze) exist in the system Nb_2O_5/WO_3. They are caused by an ordered arrangement of pentagonal tunnels filled with metal–oxygen strings. Besides the well known 4:9 phase ($Nb_8W_9O_{47}$), which has a tripled b axis, evidence for a new orthorhombic structure, $Nb_6W_8O_{39}$ ($a = b = 27.3$ Å), has been found. The oxidation products of $Nb_7W_{10}O_{47}$ and $Nb_4W_{13}O_{47}$ frequently comprise less-ordered arrangements of filled tunnels, causing diffuse scattering. In $Nb_7W_{10}O_{47.5}$ the electron diffraction patterns (along [001]) of many crystal fragments show circular diffuse scattering, which appears around the main reflections of the TTB substructure with two distinct radii (r^*). $r^* \simeq 0.33a^*$ indicates the predominance of 4:9-type domains, whereas $r^* \simeq 0.41a^*$ corresponds to $Nb_6W_8O_{39}$. In $Nb_4W_{13}O_{49}$ the diffuse scattering pattern is cross-shaped; this is due to the presence of long slabs of diamond-linked pentagonal columns. Structure models for these particular states of order have been derived from high-resolution transmission electron microscopy images. Some general principles for the formation of the different arrangements are deduced. Apparently, two distinct types of link between the filled pentagonal tunnels are important features which lead to the stability of these structures.

1. Introduction

Niobium tungsten oxides of the TTB (tetragonal tungsten bronze) type represent an excellent model system for the study of two-dimensional states of order. The underlying TTB-type substructure (Fig. 1) consists of a framework of corner-sharing MO_6 octahedra (M = Nb, W) in which tunnels are oriented along the short crystallographic axis (c axis). Three distinct types of tunnels appear, which have a trigonal, a square or a pentagonal shape when projected onto the ab plane. In TTB-type niobium tungsten oxides some of the pentagonal tunnels are filled with metal and oxygen atoms ($-O-M-O-M-$ strings). The coordination polyhedron of the cations located inside the tunnels is a MO_7 pentagonal bipyramid, which is joined by its equatorial edges to five MO_6 octahedra. The resulting structural element is designated as a pentagonal column (Lundberg *et al.*,

1982), abbreviated as PC in this paper. The TTB substructure remains almost unaltered after filling some of the pentagonal tunnels, so that the state of order is determined by the arrangement of the PC's. Since the polyhedra are connected by corner-sharing along the direction of the c axis and thereby form chains of polyhedra, the characteristic structural features appear in the ab plane. Transmission electron microscopy (TEM), therefore, provides the most powerful method for the investigation of TTB-type structures (Eyring & Tai, 1976). The arrangement of the heavy atoms can be directly imaged by high-resolution TEM (HRTEM) in projection onto the ab plane; additional information on reciprocal space can be obtained almost simultaneously by electron diffraction techniques.

Up to now, two TTB-related structures have been characterized in the pseudo-binary system Nb_2O_5/WO_3: the 4:9 phase ($Nb_8W_9O_{47}$) and the 2:7 phase ($Nb_4W_7O_{31}$). Both can be obtained by heating mixtures of the binary oxides Nb_2O_5 and WO_3 in the corresponding molar ratios 4:9 and 2:7, respectively (Roth & Waring, 1966). The preparation of the 2:7 phase requires reaction temperatures $T > 1510$ K (Roth & Waring, 1966). The 4:9 phase crystallizes in a threefold TTB superstructure ($a = a_{TTB}$, $b = 3a_{TTB}$, $c = c_{TTB}$) caused by filling 4 out of 12 pentagonal tunnels in a
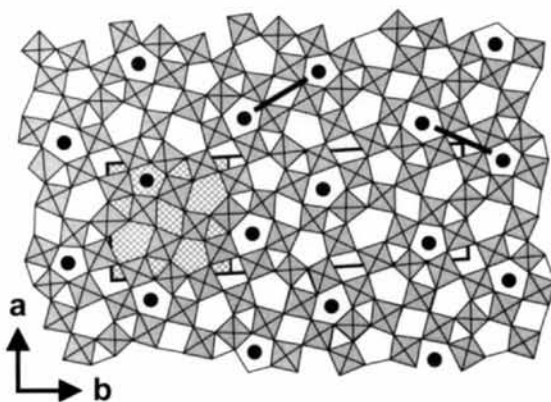

Fig. 1. Structure model of the 4:9 phase projected onto the ab plane. MO_6 octahedra (M = Nb, W) are shaded, the unit cell is outlined, a TTB subcell ($a = b = 12.2$ Å) is hatched and occupied pentagonal tunnels (pentagonal columns, PC's) are represented by filled circles. Two different orientations of diamond-linked PC pairs occur, as indicated by solid lines.

systematic way with MO strings (Fig. 1) (Sleight, 1966). Accordingly, the unit cell contains four MO strings and three TTB units ($M_{10}O_{30}$) so that the general formula is $(MO)_4(M_{10}O_{30})_3$. The MO strings are located on a fourfold position [$4(c)$ in space group $P2_12_12$ (Sleight, 1966)]. Two PC's are connected by the so-called diamond link (Lundberg *et al.*, 1982). Thereby, two orientations of the resulting PC pairs appear in the 4:9 structure (Fig. 1). The W-richer 2:7 phase (Iijima &

Allpress, 1974) crystallizes as tetragonal ($a = 2a_{TTB}$, $c = c_{TTB}$) in an intergrowth structure which comprises TTB- and ReO_3-type units (*cf.* inset in Fig. 3).

For samples with compositions in the range between the 4:9 phase (oxygen/metal ratio $O/\Sigma M = 2.765$) and the 2:7 phase ($O/\Sigma M = 2.818$), a separation into these two phases is expected that, indeed, takes part after prolonged heating at 1600 K (Iijima & Allpress, 1974). However, electron diffraction patterns of samples
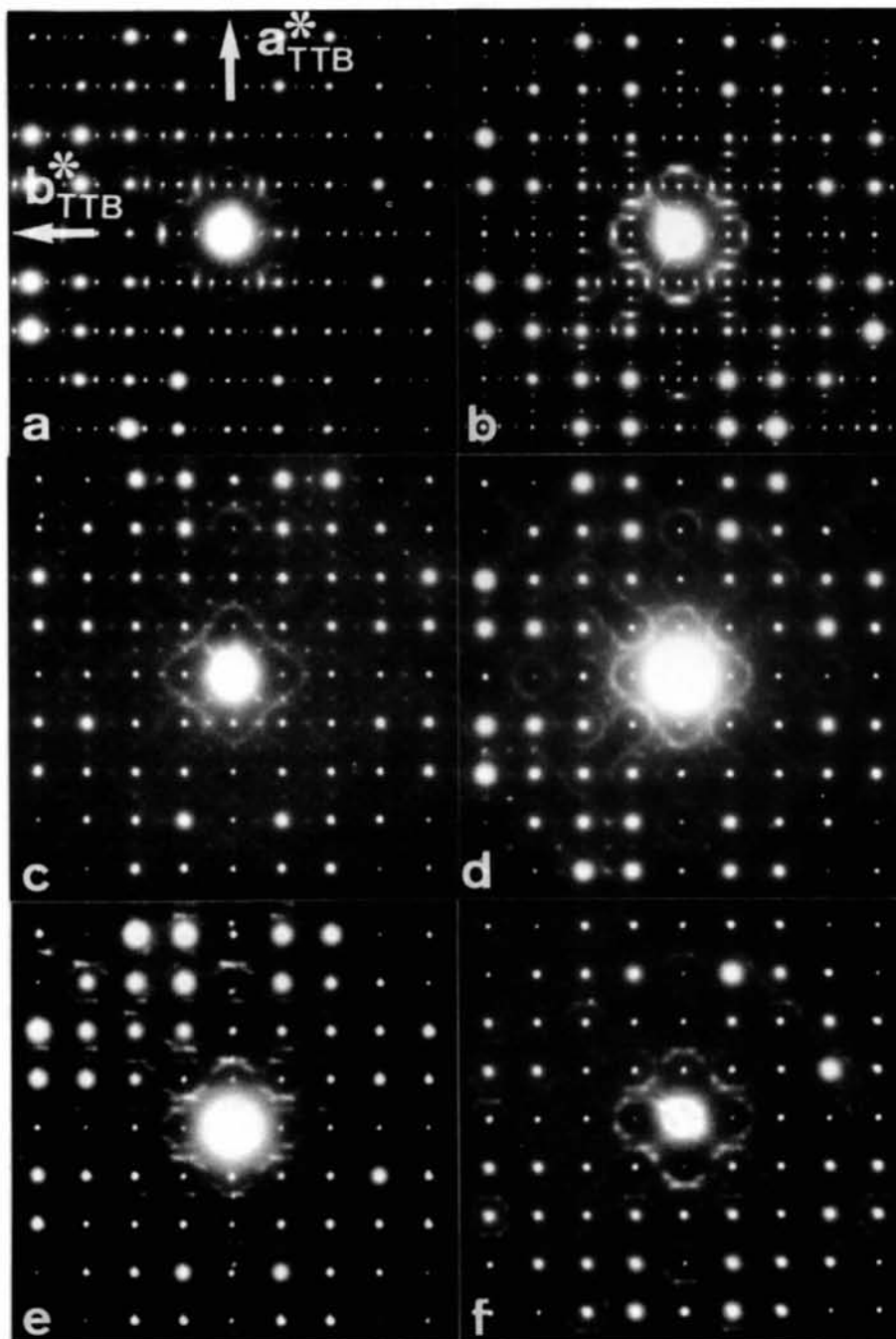

Fig. 2. $Nb_7W_{10}O_{47.5}$ ($T_{OX} = 1473$ K): SAED patterns (along [001]) of several crystallites. The Bragg reflections of the TTB matrix structure are visible as bright spots in a square arrangement. Weak spots indicate TTB superstructures and, additionally, diffuse scattering of almost circular shape appears in all patterns around the main spots with different radii r^*. (a) Threefold superstructure along b^*, $r^* \simeq 0.33a^*_{TB}$; (b) threefold superstructure along both axes, $r^* \simeq 0.33a^*_{TB}$; (c) twofold superstructure along both axes, $r^* \simeq 0.45a^*_{TB}$; (d) only circular diffuse scattering, $r^* \simeq 0.41a^*_{TB}$; (e) nonsymmetric distribution of diffuse scattering enhanced along b^*, $r^* \simeq 0.41a^*_{TB}$; (f) octagonal arrangement of additional spots, diffuse scattering between the spots.

produced by heating mixtures of the binary oxides (*e.g.* $Nb_2O_5:WO_3 = 3:8$; $O/\Sigma M = 2.786$) at lower temperatures show circular diffuse scattering around every Bragg reflection of the TTB-type sublattice (Allpress, 1969; Iijima & Cowley, 1977).

Iijima & Cowley (1977) showed that the diffuse scattering is related to short-range order in the PC sublattice. Different models for local atom configuration, so-called clusters, were successfully applied for a qualitative explanation of this scattering phenomenon in niobium tungsten oxides (Iijima & Cowley, 1977; De Ridder *et al.*, 1977; Horiuchi *et al.*, 1980). In general, diffuse scattering is correlated to an intermediate state of order [termed 'transition state' (De Ridder *et al.*, 1976; Amelinckx, 1992)] between a random arrangement and a long-range ordered structure.

A solid solution series $M_n^{4+}Nb_{8-2n}W_{9+n}O_{47}$ (M = Nb, W; $0 < n \leq 2.5$) has been characterized recently (Krumeich, Hussain *et al.*, 1995). These phases crystallize with the threefold superstructure of $Nb_8W_9O_{49}$ (Fig. 1) and they contain an amount of cations with lower valency. The TEM investigation of the oxidation
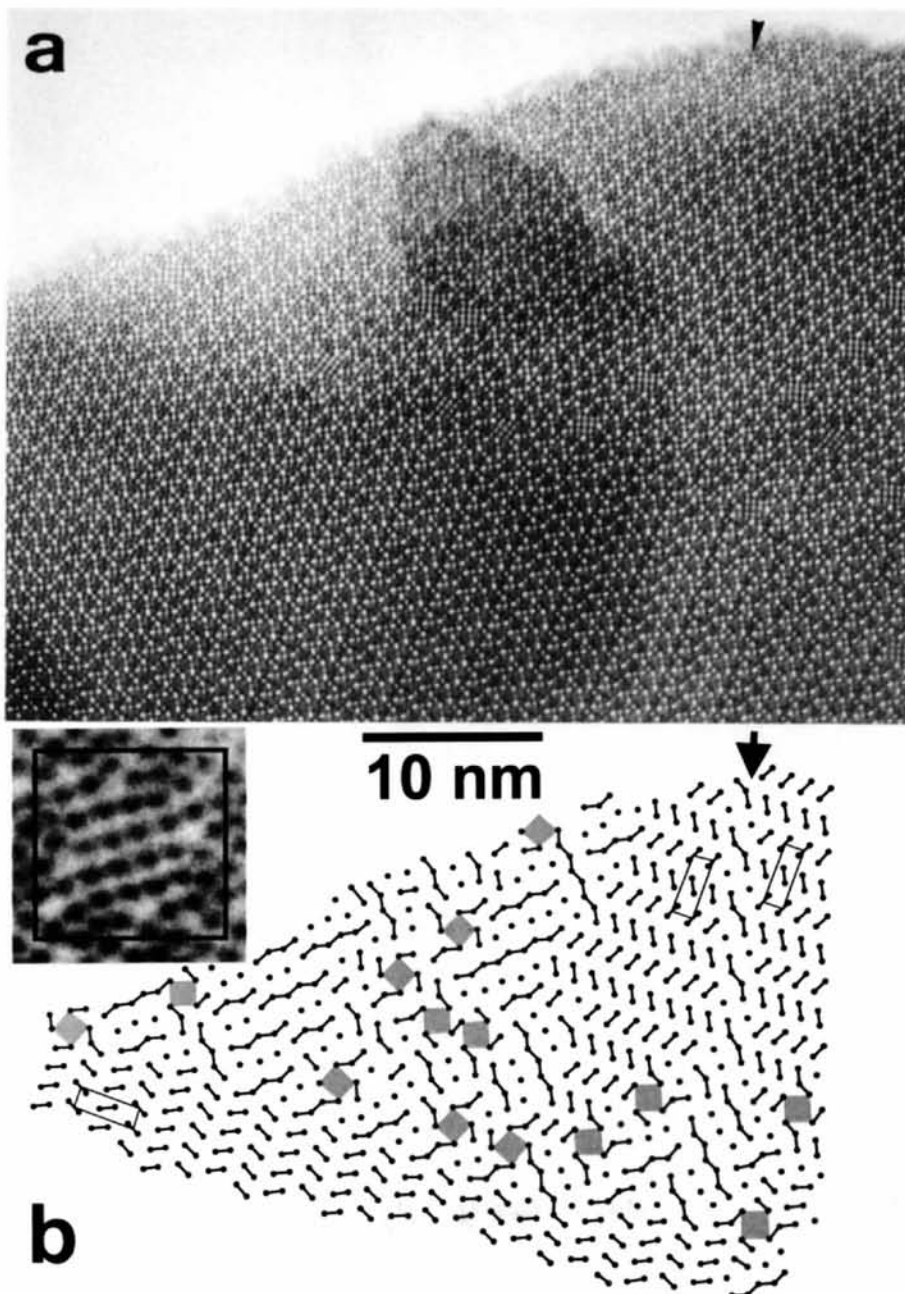

Fig. 3. $Nb_7W_{10}O_{47.5}$ (T_{OX} = 1473 K): (*a*) HRTEM image (along [001]) showing two regions of the threefold TTB superstructure as well as a disordered region in which PC slabs and single units of the 2:7 structure are present; (*b*) interpretation of the HRTEM image with the PC's symbolized by filled circles, the diamond link between PC's by a solid line and ReO₃-type arrays by grey squares. Three unit cells of the 4:9 structure are outlined. The fault boundary, causing the shift of 1/3*b* between the 4:9 structure in adjacent domains, is arrowed in (*a*) and (*b*). The HRTEM image of a unit cell (outlined) of the 2:7 structure is shown as an inset.

products of $Nb_7W_{10}O_{47}$ (Krumeich, 1995) and of $Nb_4W_{13}O_{47}$ (Krumeich, Bartsch et al., 1995) revealed the presence of interesting new structural elements and of disorder in the PC arrangement. Supplementarily to the results already published, deviating types of diffuse scattering appear in the electron diffraction patterns. This fact indicates distinguished states of order in the PC sublattice. The presented experimental results allow a comprehensive discussion of these ordering phenomena.

2. Experimental

The oxidation (on air) of $Nb_7W_{10}O_{47}$ (T_{OX} = 1473 K, 3 d) leads to $Nb_7W_{10}O_{47.5}$, and that of $Nb_4W_{13}O_{47}$ (T_{OX} = 1273 K, 3 d) leads to $Nb_4W_{13}O_{49}$, as described elsewhere (Krumeich, 1995; Krumeich, Bartsch et al., 1995).

The TEM investigations were carried out on a Philips CM30ST microscope operated at 300 kV. The samples were crushed and dispersed in acetone. Some droplets were deposited on a copper grid covered with a perforated Formvar foil (carbon coated). The grid was mounted onto a double tilt holder. Thin crystal fragments were selected and aligned along [001] by selected-area electron diffraction (SAED). The HRTEM images were recorded near the Scherzer focus so that the positions of the heavy atoms appear as dark contrasts (Horiuchi et al., 1978).

3. Results

3.1. $Nb_7W_{10}O_{47.5}$

3.1.1. *Phase separation.* For $Nb_7W_{10}O_{47.5}$, the expected separation into the 4:9 phase and the 2:7 phase occurs partly at an oxidation temperature T_{OX} = 1473 K (Krumeich, 1995). The corresponding super-structure reflections appear in the SAED patterns of several crystal fragments (Figs. 2a–c).

While the superstructure spots occur along b^* in Fig. 2(a), they are present along both axes in Fig. 2(b) due to twinning. This type of twinning, with the twinning plane being (130), is a common feature of the 4:9 phase (Eyring & Tai, 1976) and has been also observed for the starting material $Nb_7W_{10}O_{47}$ (Krumeich, Hussain et al., 1995). Furthermore, almost circular diffuse scattering (radius $r^* \simeq 0.33a^*_{TTB}$) appears centred around the basic TTB-type reflections in both SAED patterns (Figs. 2a and b). The HRTEM image (Fig. 3a) shows a thin region of the crystal fragment which gives the SAED pattern of Fig. 2(b). In order to reveal the structural details clearly, a simplified representation (Fig. 3b) shows only the essential structural features, i.e. the arrangement of the occupied pentagonal tunnels (PC's). The 4:9 structure is present in two regions; it is recognizable by characteristic rows of PC pairs oriented

parallel to the a axis (Fig. 3b). Outside these well ordered regions the crystal structure contains many faults. The unit cells of the 4:9 structure in the two regions are oriented perpendicular with respect to each other. In the 4:9-type region on the upper right side of Fig. 3 the presence of a fault boundary causes a shift of $1/3b$ between the unit cells of the adjacent domains. This shift is induced by four-membered slabs of diamond-linked PC's. Remarkably, these PC slabs are regularly arranged along the fault boundary. The boundary between the 4:9-type regions and the disordered region has a similar structure: slabs of three or more diamond-linked PC's originate from the PC pairs appearing in the 4:9 structure. Such PC slabs also occur inside the disordered region; they are up to nine PC's long and they are oriented along two perpendicular directions ([110]*_{TTB} and [1$\bar{1}$0]*_{TTB}). Furthermore, single units of the 2:7-type structure (inset in Fig. 3) occur frequently. The ReO_3-type part of this intergrowth structure is easily recognizable in the HRTEM image as square arrays of 4 × 4 dark dots. The presence of the W-richer 2:7 units, as well as the smaller amount of occupied pentagonal tunnels compared with the 4:9 structure lead to an increased $O/\Sigma M$ ratio of this area. Thus, the oxygen excess generated by the oxidation process is apparently compensated in such disordered areas.

Neither the arrangement of the PC's nor that of the 2:7 units seems to be systematic so that this disordered region contributes to the diffuse scattering. SAED patterns of crystals in which the 2:7 units are regularly arranged in large domains show the corresponding superstructure reflections (Fig. 2c). Additionally, circular diffuse scattering appears. Its radius ($r^* \simeq 0.45a^*_{TTB}$) is the largest observed yet and indicates disorder in the areas between the domains of the 2:7 structure.

However, the reflections of both superstructures, 4:9 type and 2:7 types, are absent in the SAED patterns of many crystal fragments. If this is the case, only diffuse scattering appears besides the Bragg reflections of the TTB substructure (Fig. 2d). Its shape is almost circular ($r^* \simeq 0.41a^*_{TTB}$). In Fig. 2(e) the diffuse scattering is not circular, but enhanced in the direction of the b^* axis. Remarkably, the HRTEM image (Fig. 11 in Krumeich, 1995) of the corresponding crystal fragment reveals a real structure which is quite similar to that of the disordered area in Fig. 3.

3.1.2. $Nb_6W_8O_{39}$. The electron diffraction pattern of a single-crystal fragment shows a unique octagonal arrangement of spots around every Bragg reflection of the TTB substructure (Fig. 2f). These additional spots are typical for a new TTB superstructure $M_{56}(O,F)_{156}$ (M = Mg, Nb, W), which has been found recently (Krumeich, 1997). The evaluation of the SAED pattern discloses the metrical relationship of the two pseudo-tetragonal unit cells ($a = b = 27.3$ Å) in respect of the

TTB substructure

$$a_X^* = 1/5[210]_{TTB}^*, \quad b_X^* = 1/5[\bar{1}20]_{TTB}^*$$
$$a_O^* = 1/5[2\bar{1}0]_{TTB}^*, \quad b_O^* = 1/5[120]_{TTB}^*.$$

The presence of both possible orientations of this TTB superstructure in the crystal region observed by electron diffraction results in the octagon of spots.

The corresponding HRTEM image (Fig. 4a) reveals more information about the crystal structure. Owing to a slight crystal tilt, a reliable structural interpretation is only possible in a small thin region near the crystal edge. As in the HRTEM images discussed above, PC slabs of different length as well as isolated units of the 2:7 structure are prominent structural features (Fig. 4b). The PC slabs, oriented along $[110]_{TTB}^*$ or $[1\bar{1}0]_{TTB}^*$, are up to 8 PC's long, but four-membered slabs are the most frequent. Between most of the parallel slabs more PC's are located. These PC's have no diamond link to other PC's and are termed isolated PC's for short. While the PC arrangement is only a little ordered in large parts of this region, a small well ordered microdomain of the new superstructure appears (marked in Fig. 4b, enlargement shown in Fig. 5). There, four-membered PC slabs are arranged in parallel rows with isolated PC's located in-between. This regular PC arrangement corresponds to one (X_2) of the four possible orthorhombic unit cells derived for this TTB superstructure (Fig. 6). Some of the unit cells X_1 with the PC slabs

orientated perpendicular in respect of that of X_2 are also present. Adjacent unit cells of both types (outlined in Fig. 5) demonstrate the rotational twin relationship between X_1 and X_2. Moreover, the unit cells $O_{1/2}$ and $X_{1/2}$ are related by a glide mirror operation. It should be noted that only the relative orientation of these unit cells with respect to each other can be determined by HRTEM. Owing to this close structural relationship between the four variants, twinning occurs frequently on unit-cell level, as has been discussed in detail for $M_{56}(O,F)_{156}$ (M = Mg, Nb, W) (Krumeich, 1997). Besides twinning, further faults are present, such as different slab lengths and 2:7-type units.

A unit cell of the structure model (Fig. 6) includes five TTB subcells of the composition $M_{10}O_{30}$ (M = Nb, W) and six pentagonal tunnels which are filled with MO strings. Thus, the stoichiometry can be formulated as $(MO)_6(MO_3)_{50}$. $M_{56}O_{156}$, presupposed fully oxidized cations, corresponds to $Nb_6W_8O_{39}$ ($Nb_2O_5:WO_3 = 3:8$). For this particular composition, circular diffuse scattering has been found for the first time in this system (Allpress, 1969). It should be noted that no evidence for a 2:5 structure ($Nb_4W_5O_{25}$), as proposed by Obayashi & Anderson (1976), has been found in the course of this study.

Although only a single microdomain of $M_{56}O_{156}$ has been found in the HRTEM image (Fig. 4), the presence of the superstructure reflections indicate that the larger crystal region (diameter ~0.5 μm), from which the

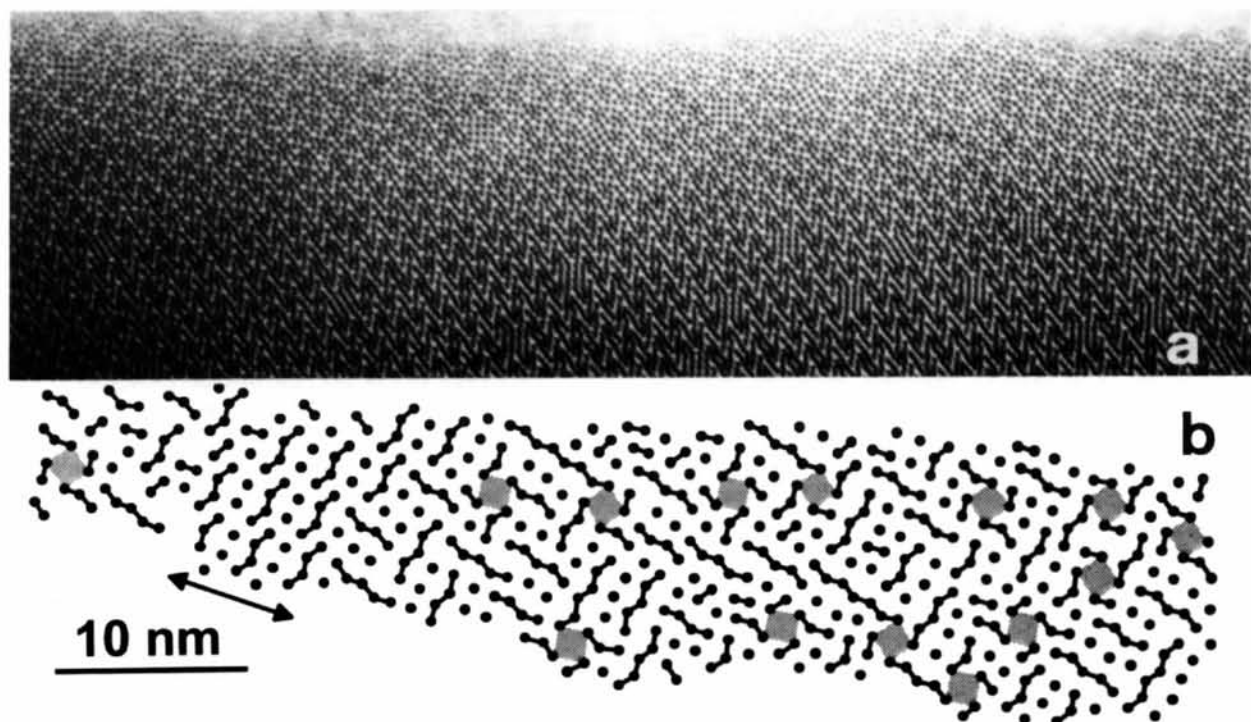Fig. 4. $Nb_7W_{10}O_{47.5}$ ($T_{OX} = 1473$ K): (a) HRTEM image (along [001]) of a region of the crystal causing the SAED pattern of Fig. 2(f); (b) interpretation of the HRTEM image (cf. Fig. 3); the arrow marks an ordered domain of $Nb_6W_8O_{39}$ (represented in Fig. 5).

SAED pattern (Fig. 2f) was taken, comprises more ordered domains.

3.2. $Nb_4W_{13}O_{49}$

The oxidation product of $Nb_4W_{13}O_{47}$ obtained at $T_{OX} = 1273$ K (Krumeich, Bartsch & Gruehn, 1995) comprises two types of crystallites. The electron diffraction patterns (along [001]) of both types show the basic reflections of the TTB substructure, as well as additional diffuse scattering. In the first type, streaking occurs along $\langle 110 \rangle^*_{TTB}$. This is caused by planar defects (orientated along $\langle 110 \rangle_{TTB}$), which are located between domains of intact TTB structure (Krumeich, Bartsch & Gruehn, 1995). In the second type of crystallite the shape of the diffuse scattering is a characteristic cross centred around the origin (Fig. 7a). The maxima of intensity are located near $\{1/2,1/2,0\}^*_{TTB}$ and near $\{3/2,1/2,0\}^*_{TTB}$. Although this shape deviates significantly from the nearly circular intensity distributions observed for $Nb_7W_{10}O_{47.5}$ (Fig. 2), the origin of diffuse scattering is presumably the presence of short-range order in the PC sublattice also. Hence, lattice imaging was applied in order to prove this assumption.

The shape of diffuse scattering in the Fourier transform (Fig. 7b) of the HRTEM image (Fig. 8a) is similar to that appearing in the SAED pattern. This correspondence shows that the diffuse scattering is also a diffraction effect of the crystal region observed by HRTEM. A simplified structural model (Fig. 8b) shows the PC arrangement derived from the HRTEM image. The Fourier transform of a point pattern (all PC's are represented by a filled circle) shows diffuse scattering (Fig. 7c), which has the same shape as in the diffractogram of the HRTEM image and is also similar to that in the SAED pattern. This fact proves the observed diffuse scattering to be decisively related to short-range order in the PC sublattice.

The PC's as well as their link-up are represented in the simplified interpretation (Fig. 8b). Thereby, details about the nature of the short-range order are clearly revealed: the predominance of long slabs of diamond-linked PC's is eye-catching. The slabs consist of up to 12 PC's and are oriented along two perpendicular $\langle 110 \rangle^*_{TTB}$ directions. In most cases a PC slab is terminated by another PC slab oriented perpendicular with respect to the first. Between two parallel slabs there are
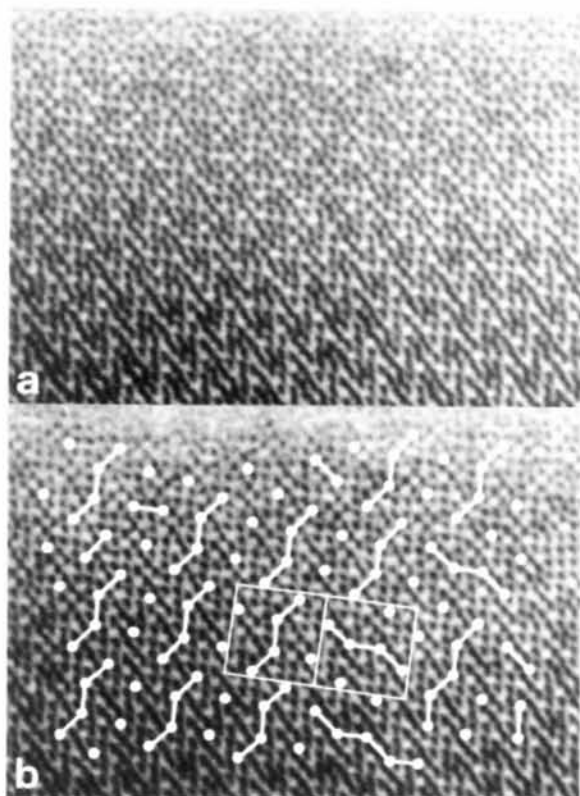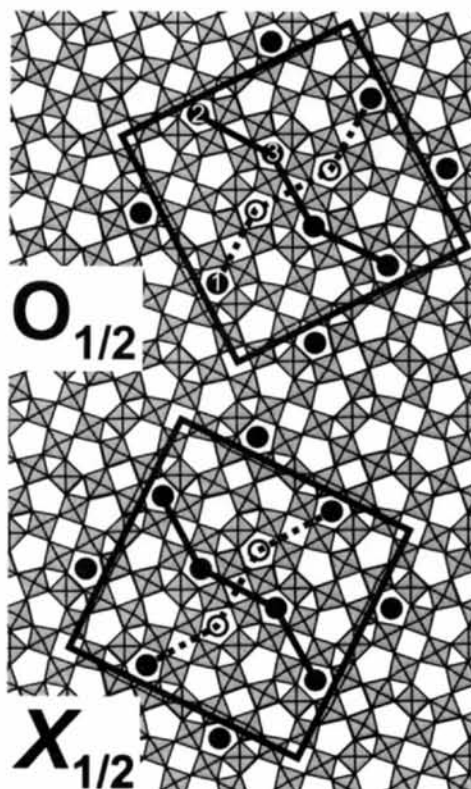

Fig. 5. (a) Enlarged region of Fig. 4(a) showing a microdomain of $Nb_6W_8O_{39}$; (b) the PC's are marked by filled circles. Two unit cells ($a = b = 27.3$ Å) are outlined, demonstrating the twin relationship between X_1 and X_2.

Fig. 6. Structure model of the new TTB superstructure viewed along **c**. Four variants of the unit cell are possible due to a different occupation of the central TTB subunit in X_1, X_2 and in O_1, O_2, respectively. Solid or open circles indicate the two possibilities of filling the four pentagonal tunnels in this unit, which leads to two possible orientations of the four-membered PC slabs in each set of unit cells. Distortions of the TTB octahedral framework by the filled pentagonal tunnels are neglected. The PC's are numbered according to Table 1.

either isolated PC's or, rarely, pairs of diamond-linked PC's. If isolated PC's are located between parallel slabs, the distance between the slabs is the same as that between the four-membered slabs in $Nb_6W_8O_{39}$ (Fig. 6). This distance along the $\langle 210 \rangle_{TTB}$ direction corresponds to the length of the a or b axis, respectively, of the fivefold TTB superstructure so that intensity at $1/5$ $\{210\}^*_{TTB}$ contributes to the diffuse scattering. A simplified structural model (Fig. 9) demonstrates the basics of the PC arrangement. If only the PC slabs are considered, the periodicity in the direction of the slabs corresponds to the diagonal of the TTB subcell (~ 17.25 Å) so that in the case of infinite parallel slabs a superstructure reflection at $(1/2,1/2,0)^*_{TTB}$ would arise. In spite of the occurrence of terminated slabs, this fact qualitatively explains the observed maximum of diffuse intensity at these sites of reciprocal space. It should be mentioned that infinite slabs of diamond-linked PC's are a common feature in several TTB-related structures. They cause the twofold TTB superstructure of $K_5Nb_9W_2O_{31}$ (Sundberg & Lundberg, 1988) and they

are present in $W_{12}O_{32}$ (Sundberg, 1978), $Nb_8W_{22}O_{86}$ and $Nb_8W_{50}O_{170}$ (Iijima, 1978).

However, although many deviations from this idealized structure model (Fig. 9) occur in the observed crystal area (Fig. 8a), such as variable slab lengths, different distances and W-richer 2:7 units, the proposed composition $(MO)_7(M_{10}O_{30})_6$ ($\sim M_{67}O_{187}$) leads to an approximate value for the ratio $O/\Sigma M = 2.791$. Remarkably, this ratio ($O/\Sigma M = 2.791$) is much less than that of $Nb_4W_{13}O_{49}$ ($O/\Sigma M = 2.882$). Thus, this arrangement apparently represents only a metastable product in which the oxidation process to $Nb_4W_{13}O_{49}$ seems to be not yet completed. On the other hand, the yellow colour of the sample indicates unambiguously the absence of reduced cations.

4. Discussion

A variety of isostructural phases crystallize with the threefold TTB superstructure of $Nb_8W_9O_{47}$ (Fig. 1): series of mixed crystals $M_n^{4+}Nb_{8-2n}W_{9+n}O_{47}$ [M = Nb, W (Krumeich, Hussain et al., 1995), Ti, Zr, Hf (Krumeich et al., 1997)] as well as $K_3Nb_{12}O_{31}F$ (Lundberg & Sundberg, 1988), and the high-temperature form of $Ta_8W_9O_{47}$ (Krumeich & Geipel, 1996) can be easily prepared. Apparently, this structure type is thermodynamically favoured for the general composition $M_{17}O_{47}$ ($O/\Sigma M = 2.765$). This extraordinary stability indicates that the interactions between the MO strings are optimized by this PC arrangement. Iijima & Allpress (1974) already postulated rules for a dense packing of MO strings in the TTB substructure:

(i) The five PT's which are directly adjacent to a PC ($d_{PC-PT} \simeq 0.6$–0.65 nm) always remain empty.

(ii) One of the two PT's having the second-nearest distance ($d_{PC-PT} \simeq 0.92$ nm) to a PC is occupied. Thereby, a pair of diamond-linked PC's results.

These rules are strictly obeyed in the 4:9-type structure, which contains the maximum number of PC's allowed by these rules. Thus, this structure constitutes the limit of possible TTB-type niobium tungsten oxides towards low $O/\Sigma M$ ratios. The related structure of the niobium-richer phase Nb_2WO_8 ($O/\Sigma M = 2.67$) consists of pentagonal columns only (Lundberg, 1972). In TTB-type niobium tungsten oxides a violation of the first rule is very uncommon and has only been observed in a few defects. It should be mentioned that the occupation of neighbouring pentagonal tunnels is a structural feature of some quaternary phases in the system Na/Nb/W/O (Sundberg & Marinder, 1990). Moreover, the second rule is strictly valid for the composition $M_{17}O_{47}$ only, as already stated by Iijima & Allpress (1974).

Since the $O/\Sigma M$ ratio of the oxidation products $Nb_4W_{13}O_{49}$ ($O/\Sigma M = 2.882$) and $Nb_7W_{10}O_{47.5}$ ($O/\Sigma M = 2.794$) is larger than that of $Nb_8W_9O_{47}$ ($O/\Sigma M = 2.765$), the oxygen excess has to be compensated structurally. Besides the formation of oxygen-richer planar defects

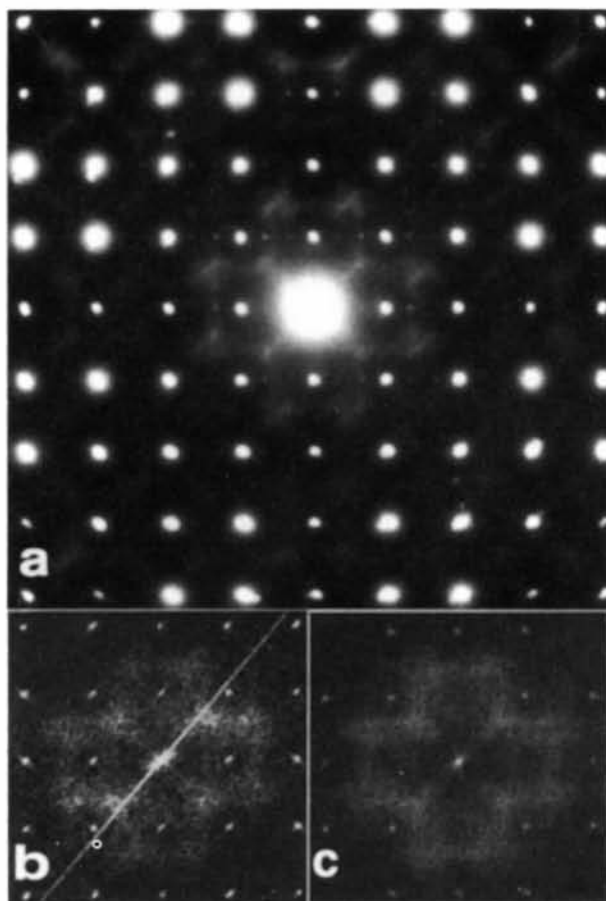Fig. 7. $Nb_4W_{13}O_{49}$ ($T_{OX} = 1273$ K): (a) SAED pattern; (b) Fourier transform of the HRTEM image (Fig. 8a) and (c) Fourier transform of the point pattern.

Table 1. *Types of PC connections (Fig. 10) and their number in the three structural models*

	$Nb_8W_9O_{47}$	$Nb_6W_8O_{39}$				$Nb_{28}W_{39}O_{187}$						
Fig.	1	6				9						
Composition	$(MO)_4(M_{10}O_{30})_3$	$(MO)_6(M_{10}O_{30})_5$				$(MO)_7(M_{10}O_{30})_6$						
$O/\Sigma M$	2.765	2.786				2.791						
PC		$2PC_1$	$2PC_2$	$2PC_3$	$\overline{PC}$	$PC_{1,2}$	PC_3	PC_4	PC_5	PC_6	PC_7	$\overline{PC}$
Type A	1	0	1	2	1	0	0	2	2	2	2	1.14
Type B	1	1	1	0	0.67	1	1	0	1	0	0	0.57
Type C	4	3	3	2	2.67	3	4	2	1	2	1	2.29

between domains of TTB structure (Krumeich, 1995; Krumeich, Bartsch & Gruehn, 1995), two distinct types of oxygen-richer structures appear:

(i) Columns of single units of the 2:7 structure ($O/\Sigma M = 2.818$) are randomly incorporated into the TTB-type structure. This also occurs for low oxidation temperatures $T_{OX} \leq 1273$ K, although the area of existence of the 2:7 phase begins at higher temperatures (Roth & Waring, 1966). The observed segregation of 4×4 blocks of corner-sharing octahedra is favoured since these blocks can be embedded coherently into the matrix structure due to the close structural relationship between the ReO_3 type and the TTB type (Hyde & O'Keeffe, 1973). However, the PC arrangement in the surrounding TTB structure is the same as in the 2:7 phase and, therefore, these segregations correspond to single units of the 2:7 structure. The presence of these W-richer units indicates local deviations of composition.

(ii) Less pentagonal tunnels of the TTB substructure are occupied than in the 4:9 phase. The composition of these oxidation products can be formulated as $(MO)_{4-x}(M_{10}O_{30})_3$. In this case the appearance of PC slabs, built up by diamond-linked PC's, is typical. This means an offence against the second rule. The formation of these PC slabs is apparently favoured compared with a random filling of pentagonal tunnels. Owing to the special geometry of the TTB structure, these PC slabs occur along two perpendicular $\langle 110 \rangle^*_{TTB}$ directions.
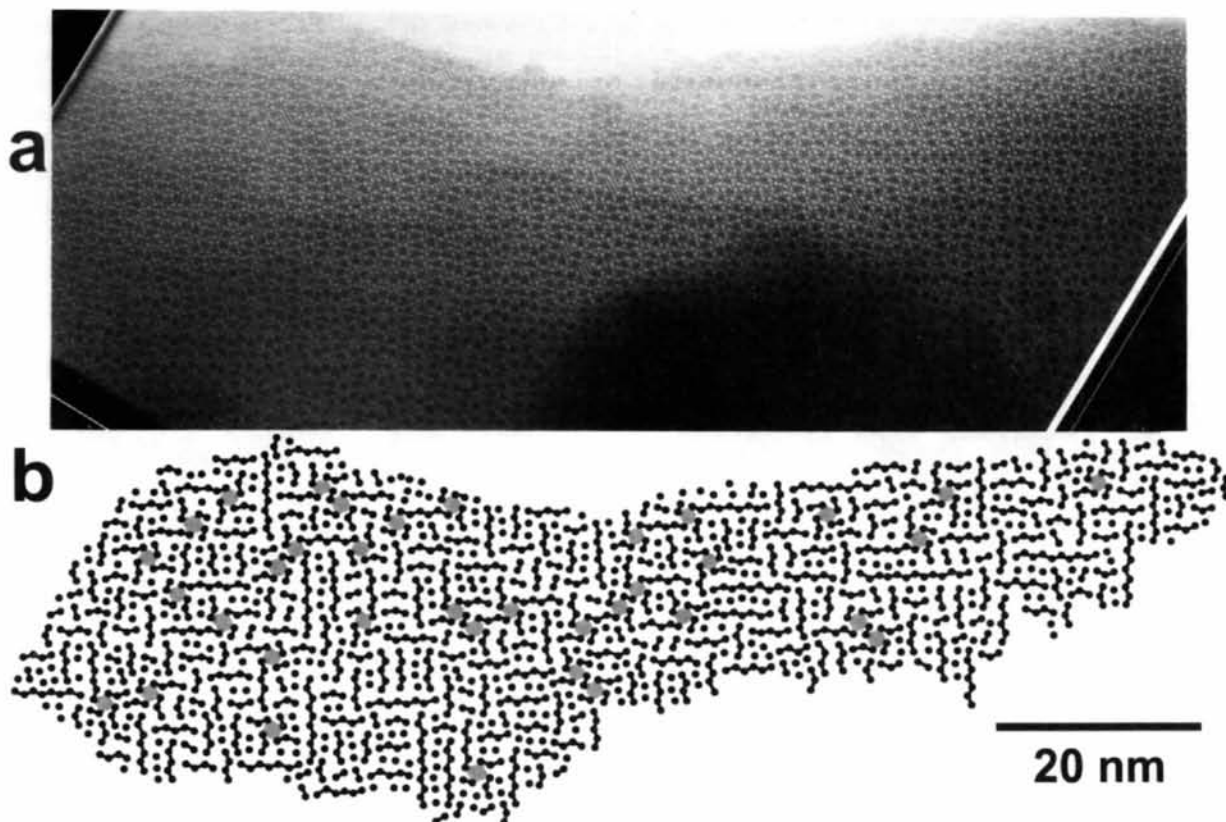

Fig. 8. $Nb_4W_{13}O_{49}$ ($T_{OX} = 1273$ K): (*a*) HRTEM image (along [001]), (*b*) interpretation (*cf.* Fig. 3).

The presented experimental results confirm that the diamond link (in the following designated as type A (Figs. 1 and 10) is important in TTB-type niobium tungsten oxides. However, in order to describe and understand the principles of the PC arrangements in these structures more comprehensively, further types (B,C) of connection between a PC and adjacent pentagonal tunnels have to be taken into account (Fig. 10): connection type A: $(d_{PC-PT} \simeq 0.92$ nm) two possibilities, diamond link; connection type B: $(d_{PC-PT} \simeq 1.15$ nm) one possibility, 2 PC's are linked via an octahedron; connection type C: $(d_{PC-PT} \simeq 1.2–1.25$ nm) eight possibilities.

In the following only the connections between filled pentagonal tunnels (PC–PC) are considered. In the 4:9 structure the PC's are located on symmetrically equivalent positions and, as a result, all PC's have the same connections to the adjacent ones: 1 A-type, 1 B-type and 4 C-type (Fig. 1, Table 1). As pointed out earlier, the PC's are arranged to pairs linked by an A-type connection. B-type connections link up these PC pairs to form rows oriented parallel to the a axis (Fig. 1).

Compared with the 4:9 structure, in which 1/3 of the pentagonal tunnels are occupied, the number of PC's is less in $Nb_6W_8O_{39}$ as well as in $(Nb,W)_{67}O_{187}$. Moreover, different sorts of PC's are present in both structures (Table 1). In $Nb_6W_8O_{39}$ (Fig. 6) three types of PC (two PC's of each sort) appear. The connections are: (i) isolated PC's: 1 B-type, 3 C-type; (ii) PC's at the end of the PC slabs: 1 A-type, 1 B-type and 3 C-type; (iii) PC's inside the slabs: 2 A-type and 2 C-type.

Consequently, the average PC $(\overline{PC})$ has 1 A-type, 2/3 B-type and 2 2/3 C-type connections (Table 1). Compared with the 4:9 structure, only the number of B-type and C-type connections of a $\overline{PC}$ is diminished. Thus, in $Nb_6W_8O_{39}$, the increase of the $O/\Sigma M$ ratio is compensated for without reducing the interactions between neighbouring MO strings much.

It should be noted that the clusters used by Iijima & Cowley (1977) for describing the short-range order in the sample $Nb_2O_5:WO_3 = 17:49$ are pairs of PC's connected by type B. While the structure of $Nb_8W_9O_{49}$ can be completely described by such PC pairs as well as by PC pairs formed by type A, both connection types have to be taken into account for a full structural description of $Nb_6W_8O_{39}$. Fig. 5(a) of Iijima & Cowley (1977) shows the interpretation of a HRTEM image of a crystal region that comprises microdomains of the 4:9 structure and of a cluster arrangement which is close to the structure of $Nb_6W_8O_{39}$. Remarkably, the 2:7 phase is completely absent in this crystal area (Fig. 3a of Iijima & Cowley, 1977), whereas all lattice images presented in this paper show several units of the 2:7 structure.

Compared with $Nb_8W_9O_{47}$ and $Nb_6W_8O_{39}$, the number of connection types B and C is considerably diminished in $(Nb,W)_{67}O_{187}$ (Table 1). This arrangement with long PC slabs obviously gains stability by increasing the amount of A-type connections.

As a general rule, all PC's in TTB-type niobium tungsten oxides have at least one A-type or one B-type connection to a neighbouring PC. With increasing $O/\Sigma M$ ratio, the density of the MO strings decreases. This is automatically combined with a decrease in the number of C-type connections; thus, this connection type is less important than the A-type and the B-type.
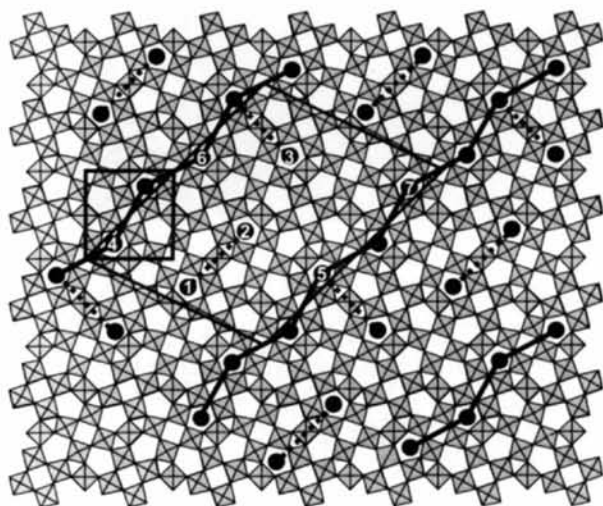

Fig. 9. Simplified structural model showing the principles of the PC arrangement in $Nb_4W_{13}O_{49}$ (Fig. 7). An area of composition $(MO)_7(M_{10}O_{30})_6$ is outlined, which contains the essential structural elements observed in the HRTEM image. A TTB subcell is outlined; the connection types A and B are symbolized by lines: A: ——— ; B: - - - -. The PC's are numbered according to Table 1.
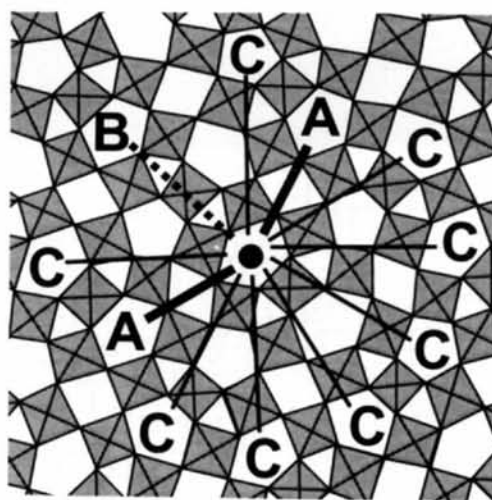

Fig. 10. For a PC in the centre of the figure, the relevant links to the adjacent pentagonal tunnels are symbolized by lines: connection type A (diamond link): ——— ; B: - - - -; C: ——— (for further explanations, see text).

5. Conclusions

While the threefold TTB superstructure of the 4:9 phase is the favourable arrangement for samples of composition $M_{17}O_{47}$ (M = Nb, W), an increase in the oxygen–metal ratio ($O/\Sigma M > 2.765$) can lead to TTB-type structures, which show little order in the PC substructure. Nevertheless, the results of the electron diffraction and the HRTEM investigations presented in this study reveal some general principles underlying these structures. In particular, slabs of diamond-linked PC's appear as structure elements in $Nb_6W_8O_{39}$ as well as in $(Nb,W)_{67}O_{187}$. In $Nb_7W_{10}O_{47.5}$, the increased $O/\Sigma M$ ratio is compensated for by forming three distinct structures: besides the well known 4:9 and 2:7 phases, evidence for a new TTB superstructure has been found. These structures occur separated or inter-grown. Additionally, diffuse scattering appearing in the electron diffraction patterns indicates short-range order in the PC arrangement. The maxima of diffuse intensity are located on circles of two different radii: $r_1^* \simeq 0.33a^*_{TTB}$ and $r_2^* \simeq 0.41a^*_{TTB}$. Understanding that diffuse scattering in this system indicates an inter-mediate state of order between a random filling of the pentagonal tunnels and a long-range ordered arrangement of PC's, one must conclude that the different radii of the circular diffuse scattering correspond to different crystal microstructures. The experimental results confirm this interpretation. $r_1^* \simeq 0.33a^*_{TTB}$ is related to the threefold TTB superstructure of the 4:9 type. In well ordered crystals the corresponding superstructure reflections (at $1/3$ a^*_{TTB}) appear along both axes, while circular diffuse scattering of radius r_1^* is still present. This type of twinning in combination with additional disorder has also been observed for the low-tempera-ture form of $Ta_8W_9O_{47}$ (Krumeich & Geipel, 1996).

Circular diffuse scattering of $r_2^* \simeq 0.41a^*_{TTB}$ had already been observed for the compositions Nb_2O_5:WO_3 = 3:8 and 17:49 (Iijima & Cowley, 1977; De Ridder et al., 1977; Horiuchi et al., 1980). Different cluster models, successfully applied for an explanation of this short-range ordered state, on the other hand, fail to predict a corresponding long-range ordered struc-ture. This structure has now been found and char-acterized: $Nb_6W_8O_{39}$ appears microtwinned, which gives rise to an octagon of superstructure spots. The edge of this octagon cuts the tetragonal axes at $0.4a^*_{TTB}$ (Fig. 2f). This value is close to the observed radius r_2^* of circular diffuse scattering. Furthermore, in several electron diffraction patterns the sites on the circles of diffuse scattering which correspond to the positions of the superstructure reflections show enhzanced intensity.

Thus, $Nb_6W_8O_{39}$ exists in the pseudo-binary system Nb_2O_5/WO_3 as a second TTB superstructure besides the 4:9 phase.

References

Allpress, J. G. (1969). *Mater. Res. Bull.* **4**, 707–720.

Amelinckx, S. (1992). *Materials Science and Technology, Vol. 2A, Characterisation of Materials*, Part. I, pp. 1–146. Weinheim: Verlag Chemie.

De Ridder, R., Van Tendeloo, G., Van Dyck, D. & Amelinckx, S. (1976). *Phys. Status Solidi A*, **38**, 663–674.

De Ridder, R., Van Tendeloo, G., Van Dyck, D. & Amelinckx, S. (1977). *Phys. Status Solidi A*, **41**, 555–560.

Eyring, L. & Tai, T.-T. (1976). *Treatise on Solid State Chemistry*, edited by N. B. Hannay, Vol. 3, pp. 167–252. New York: Plenum Press.

Horiuchi, S., Muramatsu, K. & Matsui, Y. (1978). *Acta Cryst.* A34, 939–946.

Horiuchi, S., Muramatsu, K. & Matsui, Y. (1980). *J. Appl. Cryst.* **13**, 141–147.

Hyde, B. G. & O'Keeffe, M. (1973). *Acta Cryst.* A29, 243–248.

Iijima, S. (1978). *Acta Cryst.* A34, 922–931.

Iijima, S. & Allpress, J. G. (1974). *Acta Cryst.* A30, 22–29.

Iijima, S. & Cowley, J. M. (1977). *J. Phys. Colloq.* **38**, 135–144.

Krumeich, F. (1995). *J. Solid State Chem.* **119**, 420–427.

Krumeich, F. (1997). *Z. Kristallogr.* **212**, 708–711.

Krumeich, F., Bartsch, C. & Gruehn, R. (1995). *J. Solid State Chem.* **120**, 268–274.

Krumeich, F. & Geipel, T. (1996). *J. Solid State Chem.* **124**, 58–64.

Krumeich, F., Hussain, A., Bartsch, C. & Gruehn, R. (1995). *Z. Anorg. Allg. Chem.* **621**, 799–806.

Krumeich, F., Liedtke, G. & Mader, W. (1997). *Z. Anorg. Allg. Chem.* **623**, 990–996.

Lundberg, M. (1972). *Acta Chem. Scand.* **26**, 2932–2940.

Lundberg, M. & Sundberg, M. (1988). *J. Less-Common Met.* **137**, 163–179.

Lundberg, M., Sundberg, M. & Magnéli, A. (1982). *J. Solid State Chem.* **44**, 32–40.

Obayashi, H. & Anderson, J. S. (1976). *J. Solid State Chem.* **17**, 79–89.

Roth, R. S. & Waring, J. L. (1966). *J. Res. Natl Bur. Stand. Sect. A*, **70**, 281–303.

Sleight, A. W. (1966). *Acta Chem. Scand.* **20**, 1102–1112.

Sundberg, M. (1978). *Chem. Scr.* **14**, 161–166.

Sundberg, M. & Lundberg, M. (1988). *Chem. Scr.* **28**, 77–80.

Sundberg, M. & Marinder, B.-O. (1990). *J. Solid State Chem.* **84**, 23–38.